EPR study of Gd^{3+} centres in Tl_2ZnF_4 crystals

2003 J. Phys.: Condens. Matter 15 3779

(http://iopscience.iop.org/0953-8984/15/22/312)

INSTITUTE OF PHYSICS PUBLISHING JOURNAL OF PHYSICS: CONDENSED MATTER

J. Phys.: Condens. Matter **15** (2003) 3779–3792 PII: S0953-8984(03)57460-4

EPR study of Gd^{3+} centres in Tl_2ZnF_4 crystals

M Arakawa[1], T Nakano[1], H Ebisu[2] and H Takeuchi[3]

[1] Department of Materials Science and Engineering, Nagoya Institute of Technology, Nagoya 466-8555, Japan
[2] Department of Electrical and Computer Engineering, Nagoya Institute of Technology, Nagoya 466-8555, Japan
[3] Department of Advanced Science and Technology, Toyota Technological Institute, Nagoya 468-8511, Japan

Received 13 December 2002, in final form 3 April 2003
Published 23 May 2003
Online at stacks.iop.org/JPhysCM/15/3779

Abstract

EPR measurements have been made at room temperature on Tl_2ZnF_4 crystals doped with Gd^{3+} and co-doped with Gd^{3+} and Li^+. For crystals doped only with Gd^{3+}, a spectrum with tetragonal symmetry (A centre) is observed. For co-doped crystals new spectra with tetragonal (B centre) and monoclinic (C centre) symmetries are observed in place of the spectrum of the A centre. The A centre is identified as the substitutional Gd^{3+} ion at a Zn^{2+} site in six-fold coordination without any local charge compensation in its immediate neighbourhood. On the basis of spin Hamiltonian separation analysis, the separated parameter $b_{2a(1)}$ for the C centre has a value close to the b_2^0 parameter for the B centre. The B and C centres in co-doped crystals are ascribed to a Gd^{3+} ion substituted for a Tl^+ site in nine-fold coordination, where the divalent excess positive charge on Gd^{3+} is compensated by a Li^+ ion at the Zn^{2+} site along the c axis. For the C centre, another association with a Li^+ ion is found at the nearest Zn^{2+} site along the [111] direction. The other separated parameter $b_{2a(2)}$ for the C centre has an opposite sign and six times the magnitude of b_2^0 for the Gd^{3+} centre with trigonal symmetry along the [111] direction in $RbCaF_3$. The large magnitude negative value may be due to the deviation of the ligands toward the Li^+ ion at the nearest Zn^{2+} site.

1. Introduction

The structure of K_2NiF_4-like layered perovskite crystals with space group $I4/mmm$ may be regarded as a two-dimensional network of NiF_6 octahedra, in contrast with the three-dimensional network in the structure of $KNiF_3$-like cubic perovskite crystals. EPR spectra of the trivalent Gd^{3+} ions in layered perovskite A_2BF_4 crystals [1, 2] have been studied by comparing them with those in cubic perovskite ABF_3 crystals [3–5]. In A_2BF_4 crystals, it is important to know the relationship between the fine-structure parameters b_n^m in the spin

Hamiltonian and the local environment around the magnetic ions for identification of the centres associated with nearby charge compensators.

The superposition model proposed by Newman [6] has been applied extensively to the ground multiplet splittings of $3d^5$ and $4f^7$ ions on analysis of the local environment [7]. However, the number of independent fitting parameters, such as ligand positions, are much more than the number of fine-structure parameters. So, the superposition model may not be successful without some model for the distorted ligand configuration by a charge compensator in tetragonal A_2BF_4 crystals.

The information on the local environments of Gd^{3+} centres in A_2BF_4 was successfully obtained using the spin Hamiltonian separation method [1, 8]. The spin Hamiltonian separation method is based on the separation of the local environment, including a charge compensator, into two configurations with axial symmetry. In this method, the relationships between the fine-structure parameters b_n^m and the local environments around magnetic ions were deduced by separating the fine-structure terms into two uniaxial terms along the c axis and along the direction to the charge compensator. For the former a parameter $b_{2a(1)}$ corresponds to the configuration similar to that for the centre without any local charge compensator nearby in a A_2BF_4 crystal, and for the latter a parameter $b_{2a(2)}$ corresponds to the configuration similar to that for the charge-compensated centre of the same kind in a cubic ABF_3 crystal. Each separated parameter was found to give systematic information on the axial parameter for the uncompensated centre in a A_2BF_4 crystal and on the axial parameter for the same kind of centre in a ABF_3 crystal, enough to identify the charge-compensated centre in A_2BF_4 unambiguously.

In ABF_3 crystals composed of divalent cations (B = Cd, Ca) having ionic radii close to that of the Gd^{3+} ion, a Gd^{3+} ion substitutes for a host divalent cation in six-fold coordination [3–5, 9–11]. In layered perovskite fluorides A_2CdF_4 (A = Rb, Cs) [1, 2], a Gd^{3+} ion substitutes for a Cd^{2+} ion, similar to the case for $ACdF_3$ host crystals. In these crystals the Gd^{3+} centres with tetragonal symmetry (the I centre) were observed [1]. On the basis of spin Hamiltonian separation analysis, the separated parameters $b_{2a(1)}$ for the charge-compensated centre in the same host crystals have a value close to the b_2^0 parameter for the I centre [1]. This indicates that the I centre is ascribed to a Gd^{3+} without any local charge compensation in its immediate neighbourhood (denoted as the uncompensated centre hereafter).

On the other hand, in cubic perovskite fluorides $KMgF_3$ [12], $KZnF_3$ [9] and $RbZnF_3$ [13] with divalent cations having ionic radii smaller than that of the Gd^{3+} ion, a Gd^{3+} ion substitutes for a monovalent cation in twelve-fold coordination without any local charge compensation nearby in spite of the excess doubly positive charge on the Gd^{3+}. For K_2MgF_4 and K_2ZnF_4, no EPR spectrum of the Gd^{3+} ion has been observed. In Rb_2ZnF_4 [2], signals from the Gd^{3+}–O^{2-} pair replacing a Zn^{2+}–F^- bond were observed without those from the I centre, contrary to the case for A_2CdF_4 (A = Rb, Cs) crystals [1], where signals from the I centre were observed with large intensity.

It is well known in ABF_3 crystals that the structure is classified by the tolerance factor $t\ (= (r_A+r_F)/\sqrt{2}(r_B+r_F))$. The cubic perovskite structure occurs in the range $0.88 \leqslant t \leqslant 1.00$ and the hexagonal $BaTiO_3$-type structure in the range $1.00 \leqslant t \leqslant 1.06$ [14]. On the other hand, A_2BF_4 crystals keep the layered perovskite structure over the range of the tolerance factor corresponding to the cubic and hexagonal structures of ABF_3 crystals. Crystals of Tl_2ZnF_4 ($t = 1.01$) have the layered perovskite structure, in contrast with the hexagonal one for that of $TlZnF_3$. Figure 1 shows the unit cell of Tl_2ZnF_4. On the basis of spin Hamiltonian separation analysis, we can obtain the information on the charge-compensated centres formed in the virtual cubic perovskite crystal of $TlZnF_3$ in figure 1(a) from the separated parameters for the centres observed in Tl_2ZnF_4. Recently, anomalies were revealed in the separated parameters for Cr^{3+} centres of several kinds in Tl_2ZnF_4 crystals, which have about double the magnitude of

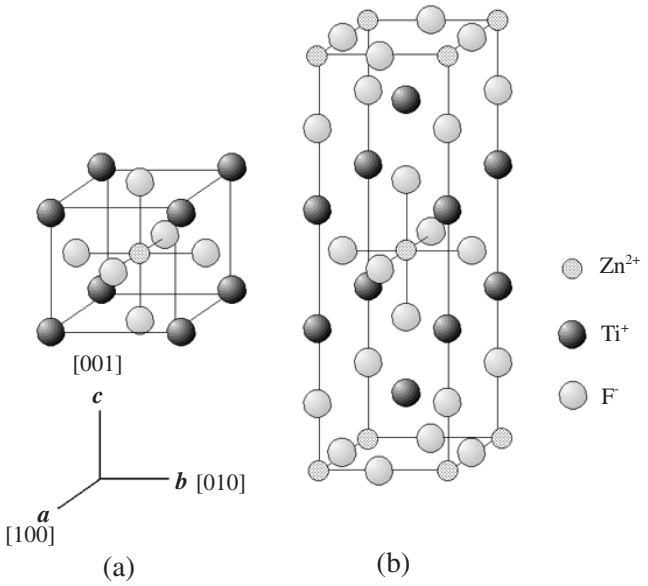

Figure 1. Unit cells of (a) a virtual cubic perovskite $TlZnF_3$ crystal and (b) a layered perovskite Tl_2ZnF_4 crystal.

those in the other layered perovskite fluorides K_2ZnF_4 and Rb_2ZnF_4 with different monovalent cations [15].

In this paper, we will report EPR results for the Gd^{3+} centres observed in Tl_2ZnF_4 single crystals. For crystals doped with Gd^{3+}, a spectrum with tetragonal symmetry is observed. For crystals co-doped with Gd^{3+} and Li^+, new spectra with tetragonal and monoclinic symmetries are observed in place of that for the tetragonal centre observed in the Gd^{3+}-only doped crystals. The monoclinic centre will be analysed using the spin Hamiltonian separation method. The local environments around the Gd^{3+} ions will be discussed by the separated parameters.

2. Experimental procedure

Single crystals of Tl_2ZnF_4 were grown in graphite crucibles by the Bridgman technique. Gd metal (99.9%) was added to starting mixtures of ZnF_2 and TlF. In crystals co-doped with Gd^{3+} and Li^+, powdered LiF was added to the mixture. The crystals obtained are cleaved easily in the c plane. The measurements were made using a JES-FE1XG ESR spectrometer operating in the X-band at the Centre for Instrumental Analysis at Nagoya Institute of Technology.

3. Results

Signals from a magnetic centre with $S = 7/2$ (hereafter called the A centre) were observed for a Tl_2ZnF_4 crystal doped with Gd^{3+} ions. A recorder trace of the EPR signals with $\boldsymbol{H} \parallel a$ at room temperature is shown in figure 2(a). Figure 2(b) shows the recorder trace of EPR signals for another crystal co-doped with Gd^{3+} and Li^+. For co-doped crystal, new signals from centres of two kinds (hereafter called the B and C centres) appear in place of those from the A centre, as seen from figure 2. The signals from the A, B and C centres are marked with roman capitals in the figure.

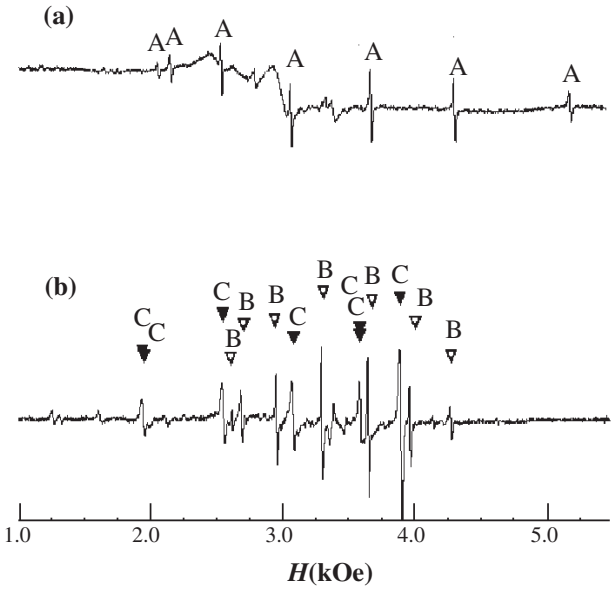

Figure 2. EPR spectra of Gd^{3+} centres observed at room temperature with $\boldsymbol{H} \parallel a$ in Tl_2ZnF_4 (a) doped only with Gd^{3+} and (b) co-doped with Gd^{3+} and Li^+. The roman capitals A, B and C denote the signals from the A, B and C centres, respectively.

In figure 3 signals from the A centre observed at room temperature are plotted by open circles against external field direction in the *c* plane. The angular variations of their resonance fields show dependences of 90° periodicity in this plane. The field direction of the minimum fine-structure spread in figure 3 is determined to be parallel to the crystalline axis in the *c* plane. The total spread of the fine-structure signals is a maximum in the [001] direction. These results indicate that the spectrum of the A centre has tetragonal symmetry about the crystalline *c* axis.

In figure 4 signals observed are plotted against external field direction in the *c* plane by full squares for the B centre and by open circles for the C centre. As seen from figure 4, the signals from the B centre show dependences of 90° periodicity, similar to those from the A centre in figure 3. This indicates that the spectrum of the B centre has also tetragonal symmetry about the crystalline *c* axis, although the fine-structure splitting for the B centre is about one half the magnitude of that for the A centre.

The spectrum of the A and B centres can be described by the following spin Hamiltonian with tetragonal symmetry;

$$\mathcal{H} = g\beta \boldsymbol{S} \cdot \boldsymbol{B} + \tfrac{1}{3} b_2^0 O_2^0 + \tfrac{1}{60}[b_4^0 O_4^0 + b_4^4 O_4^4] + \tfrac{1}{1260}[b_6^0 O_6^0 + b_6^4 O_6^4] \qquad (1)$$

where O_2^0, O_4^0, O_4^4, O_6^0 and O_6^4 are the Stevens operators defined by Abragam and Bleaney [16]. The Zeeman term is assumed to be isotropic, similar to that obtained previously for Gd^{3+} centres in several host crystals. The spin Hamiltonian is described in the coordination system where the principal *z* axis is chosen to be parallel to the crystalline *c* axis. The *x* axis is chosen to be parallel to the crystalline *a* axis.

The signals from the C centre have a set of branches as shown in figure 4. The branches, which have peaks and troughs in the [110] direction, coincide with each other in the [100] and [010] directions. From the field-direction dependence in the $(\bar{1}10)$ plane we see two kinds of branches as shown in figure 5. One shows extremes for a direction declined by about 40° from the *c* axis in the plane. The other shows extremes in the [110] direction. The different kinds

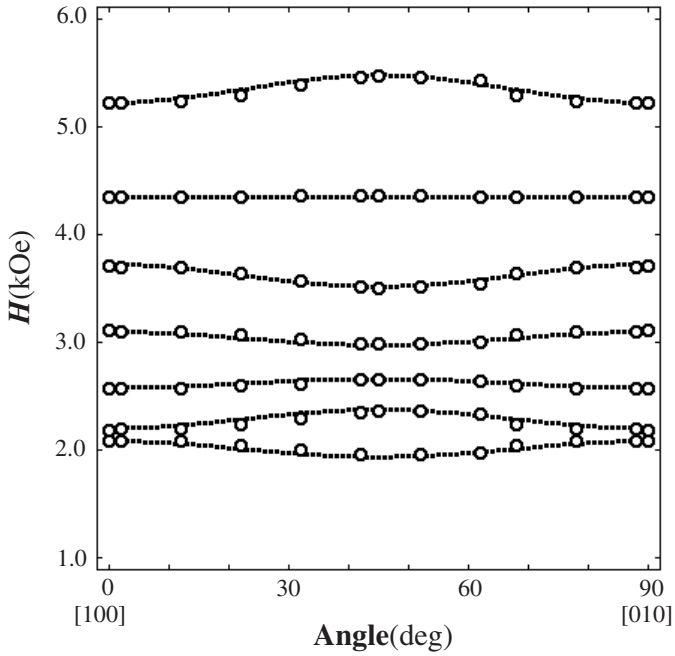

Figure 3. Angular variation of the signals labelled A in figure 2(a) with $\boldsymbol{H}$ in the c plane. Open circles denote the resonance fields observed for the A centre and dotted curves denote the calculated resonance fields using the parameters listed in table 1.

of branches coincide with each other in the [001] direction. From this feature of the branches the main principal axis (z axis) of the C centre is considered to be declined from the c axis toward a $\langle 110 \rangle$ direction. This makes it clear that the spectra of the C centre have monoclinic symmetry. Each branch corresponds to the association of some charge compensator in one of the $\langle 110 \rangle$ symmetry planes.

The spectra of the C centre were well fitted within experimental errors to the following spin Hamiltonian:

$$\mathcal{H} = g\beta \boldsymbol{S} \cdot \boldsymbol{B} + \tfrac{1}{3}[b_2^0 O_2^0 + b_2^2 O_2^2] + \tfrac{1}{60}[b_4^0 O_4^0 + b_4^2 O_4^2 + b_4^3 O_4^3 + b_4^4 O_4^4] + \tfrac{1}{1260}[b_6^0 O_6^0 + b_6^2 O_6^2 + b_6^3 O_6^3 + b_6^4 O_6^4 + b_6^6 O_6^6]. \quad (2)$$

The z axis in the spin Hamiltonian is chosen to be the direction declined at an angle θ from the c axis in the $(\bar{1}10)$ symmetry plane, where the $b_2^1 O_2^1$ term vanishes. The x axis is chosen in the same plane. The isotropic Zeeman term is assumed similarly to those for the A and B centres.

The spectra observed were fitted to the spin Hamiltonian by the matrix diagonalization method. From the fitting of the spin Hamiltonian parameters for the EPR spectra, only the relative signs among b_n^m parameters can be uniquely determined. The absolute signs of the parameter b_n^m for the A and B centres were determined by the response of the cubic components of the crystal field to the fine-structure parameter, to be mentioned in the following section 4.1. The spin Hamiltonian parameters obtained for the A and B centres are listed in table 1.

For the C centre the spin Hamiltonian parameters and the angle θ listed in table 2 are obtained by the matrix diagonalization method. The absolute signs of b_n^m and θ for the C centre were determined by the spin Hamiltonian separation analysis. Details will be mentioned in the

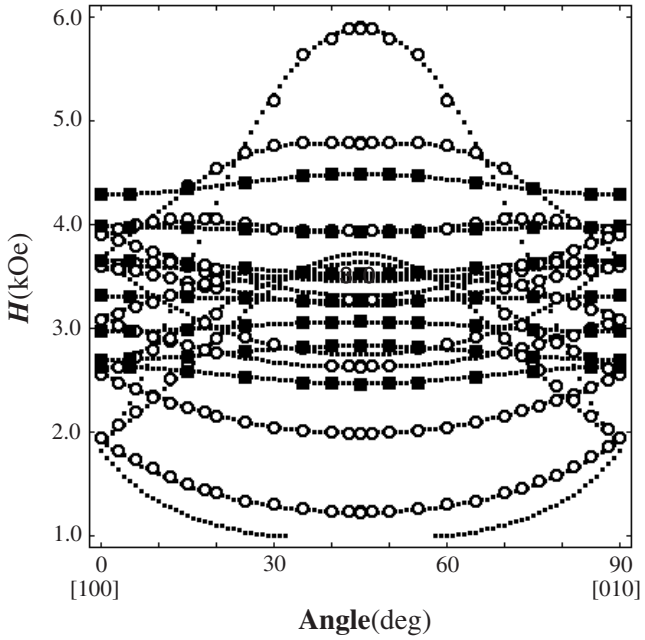

Figure 4. Angular variation of the signals B and C in figure 2(b) with $\boldsymbol{H}$ in c plane. Full squares are due to the B centre and open circles are due to the C centre. Dotted curves denote the calculated resonance fields using the parameters for the B and C centres listed in tables 1 and 2. Weak signals corresponding to the lowest-field branch for the C centre are not recognized in this plane by the appearance of unknown forbidden-like signals.

Table 1. Spin Hamiltonian parameters for the A and B centres with tetragonal symmetry observed in Tl_2ZnF_4. The units are 10^{-4} cm^{-1} for b_n^m.

Crystal	Centre	g	b_2^0	b_4^0	b_4^4	b_6^0	b_6^4
Tl_2ZnF_4	A	1.992(1)	−557.6(5)	−3.8(1)	−47.9(5)	0.8(1)	−18.6(2)
	B	1.992(1)	−288.9(4)	1.1(1)	−36.3(7)	0.4(2)	−2.0(2)

Table 2. Spin Hamiltonian parameters for the C centre observed in Tl_2ZnF_4 in the coordination system where the $b_2^1 O_2^1$ term vanishes. The value of θ is the angle between the c axis and the z axis in the spin Hamiltonian. The units are 10^{-4} cm^{-1} for b_n^m.

g	b_2^0	b_2^2	b_4^0	b_4^2	b_4^3	b_4^4
1.992(1)	−465.7(7)	−256.7(6)	0.0(3)	7.1(8)	51(4)	27(1)
	b_6^0	b_6^2	b_6^3	b_6^4	b_6^6	θ (deg)
	0.1(4)	0(2)	−9(4)	−2(2)	8(3)	40.28(6)

following section 4.2. Dotted curves in figures 3–5 show the theoretical curves calculated using the spin Hamiltonian parameters listed in tables 1 and 2. Good agreement of the calculated values of resonance fields with experimental ones is obtained.

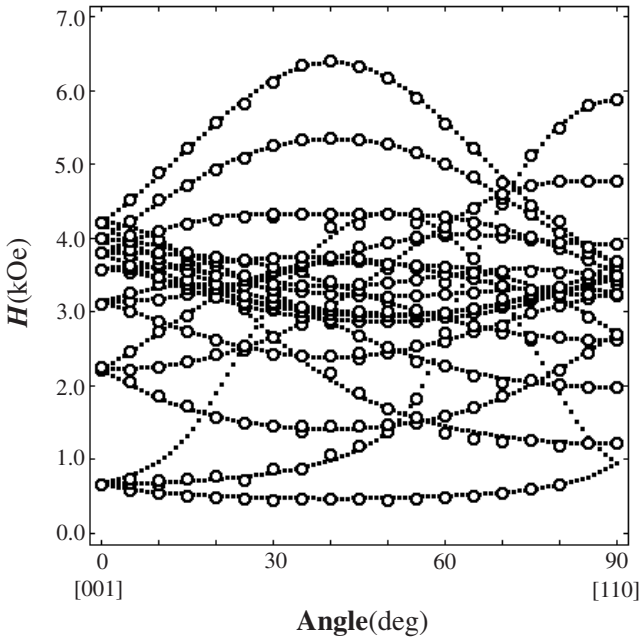

Figure 5. Angular variation of the spectra of the C centre with $\boldsymbol{H}$ in the $(\bar{1}10)$ plane. Open circles show the signals observed. Dotted curves denote the calculated resonance fields using the parameters for the C centre listed in table 2.

4. Discussions

4.1. Tetragonal centres A and B

The ionic radii of a Cd^{2+} ion (0.97 Å) and a Ca^{2+} ion (0.99 Å) are almost the same as that of the Gd^{3+} ion (0.97 Å), in contrast with the smaller ones of Mg^{2+} (0.66 Å) and Zn^{2+} (0.74 Å). In cubic perovskite fluorides $KMgF_3$ [12], $KZnF_3$ [9] and $RbZnF_3$ [13], a Gd^{3+} ion substitutes for a monovalent cation in twelve-fold coordination without any local charge compensation in spite of the excess doubly positive charge on the Gd^{3+}. On the other hand, no EPR spectrum of a Gd^{3+} ion at a monovalent cation site has been observed in layered perovskite fluorides K_2MgF_4, K_2ZnF_4 and Rb_2ZnF_4.

The fine structure terms to the fourth-rank and sixth-rank Stevens operators for the tetragonal centres are known to be represented by uniaxial and cubic terms as follows:

$$\tfrac{1}{60}[b_4^0O_4^0 + b_4^4O_4^4] = \tfrac{1}{60}[b_{4a}O_4^0 + b_{4c}(O_4^0 + 5O_4^4)], \tag{3}$$

and

$$\tfrac{1}{1260}[b_6^0O_6^0 + b_6^4O_6^4] = \tfrac{1}{1260}[b_{6a}O_6^0 + b_{6c}(O_6^0 - 21O_6^4)]. \tag{4}$$

Equations (3) and (4) are valid when the following conditions are satisfied:

$$b_{4a} = b_4^0 - \tfrac{1}{5}b_4^4, \qquad b_{4c} = \tfrac{1}{5}b_4^4, \tag{5a}$$

$$b_{6a} = b_6^0 + \tfrac{1}{21}b_6^4, \qquad b_{6c} = -\tfrac{1}{21}b_6^4. \tag{5b}$$

Values of the parameters $b_{2a}(= b_2^0)$, b_{na} and b_{nc} $(n = 4, 6)$ for the A and B centres calculated by equations (5) are listed in table 3 together with those for the I centre in Rb_2CdF_4 and Cs_2CdF_4 for comparison. The terms in b_{4c} and b_{6c} denote the cubic character of the centre.

Table 3. Fine-structure parameters b_{na} and b_{nc} for the Gd^{3+} A and B centres with tetragonal symmetry observed in Tl_2ZnF_4 together with those for the I centres reported in other layered perovskite fluorides. The units are 10^{-4} cm^{-1} for the fine-structure parameters.

Crystal	Centre	a (Å)	c (Å)	b_{2a}	b_{4a}	b_{4c}	b_{6a}	b_{6c}
K_2MgF_4	—	3.9704	13.176 [17]	—	—	—	—	—
K_2ZnF_4	—	4.0548	13.096 [17]	—	—	—	—	—
Tl_2ZnF_4	A	4.105	14.10 [14]	−557.6	5.78	−9.58	−0.09	0.89
	B			−288.9	8.36	−7.26	0.30	0.10
Rb_2ZnF_4	—	4.136	13.706 [17]	—	—	—	—	—
Rb_2CdF_4	I [1]	4.4017	13.938 [17]	−549.9	5.25	−8.64	−0.02	0.85
Cs_2CdF_4	I [1]	—	—	−443.0	6.55	−9.92	−0.06	0.94

The cubic parameters b_{4c} have been known empirically to have negative signs for Gd^{3+} in six-, eight- and twelve-fold coordinations [3]. This suggests a negative sign for the parameter b_4^4, by equation (5*a*). We therefore conclude that signs of b_n^m in table 1 are appropriate.

It has been known empirically that the parameters b_{4c} and b_{6c} have different magnitudes in the different ligand coordinations [13]. On the basis of spin Hamiltonian separation analysis, the I centre was ascribed to the uncompensated Gd^{3+} centre. The b_{4c} and b_{6c} for the A centre have values close to those for the I centre in Rb_2CdF_4 and Cs_2CdF_4 as seen from table 3. The result indicates that the A centre is ascribed to a Gd^{3+} ion at a Zn^{2+} site in six-fold coordination without any local charge compensation in its immediate neighbourhood. The axial parameters b_{na} ($n = 2, 4, 6$) in table 2 are also comparable with those for the I centres previously reported. This fact supports the conclusion that the A centre is the same uncompensated centre as the I centre observed in Rb_2CdF_4 and Cs_2CdF_4. A schematic model of the A centre is shown in figure 6(a). This may be the first observation of the Gd^{3+} ion substituted for a Zn^{2+} ion in layered perovskite fluorides without any charge compensator in its immediate neighbourhood.

For Rb_2ZnF_4, signals from a Gd^{3+}–O^{2-} pair replacing a Zn^{2+}–F^- bond in the c plane was observed without those from the I centre. The substitution of Gd^{3+} for Zn^{2+} may be allowed by the presence of O^{2-} at the ligand site on the crystalline a or b axes. The elongated ligand octahedron along the c axis makes it possible for a Gd^{3+} ion to substitute for Zn^{2+}, since the space for the Gd^{3+} is enlarged by the Coulomb repulsion between the O^{2-} ion and the ligand F^- ions along the c axis. The elongation of the ligand octahedron was confirmed, on the basis of spin Hamiltonian separation analysis, by the fact that the separated parameter $b_{2a(1)}$ changes its sign from negative for the Gd^{3+}–V_{Cd} and the Gd^{3+}–Li^+ centres in A_2CdF_4 [1] to positive for the Gd^{3+}–O^{2-} centres in A_2CdF_4 (A = Rb, Cs) [2] and Rb_2ZnF_4 [2].

As shown in table 3 the lattice parameter c along the c axis in Tl_2ZnF_4 is larger than that in Rb_2ZnF_4, although the ionic radius of Tl^+ (1.47 Å) is the same as that of Rb^+ (1.47 Å). Recently, anomalously large fine-structure splittings were observed for the uncompensated Cr^{3+} centres in Tl_2MgF_4 and Tl_2ZnF_4 crystals, which were about double the magnitude of those in the other layered perovskite fluorides K_2MF_4 and Rb_2MF_4 (M = Mg, Zn) [15, 18]. The anomaly may also be related to the enlarged space along the c axis. As seen from table 3, the lattice parameter c in Tl_2ZnF_4 is almost the same as that in Rb_2CdF_4 [1], where the Gd^{3+} substitutes for Cd^{2+} in six-fold coordination. The enlarged space of the Zn^{2+} site along the c axis makes it possible for a Gd^{3+} ion to substitute for a Zn^{2+} ion in six-fold coordination in Tl_2ZnF_4.

The parameters b_{4c} and b_{6c} are known empirically to be characteristic of coordination number for Gd^{3+} in perovskite-like fluorides [13]. Contrary to the A centre, values of the

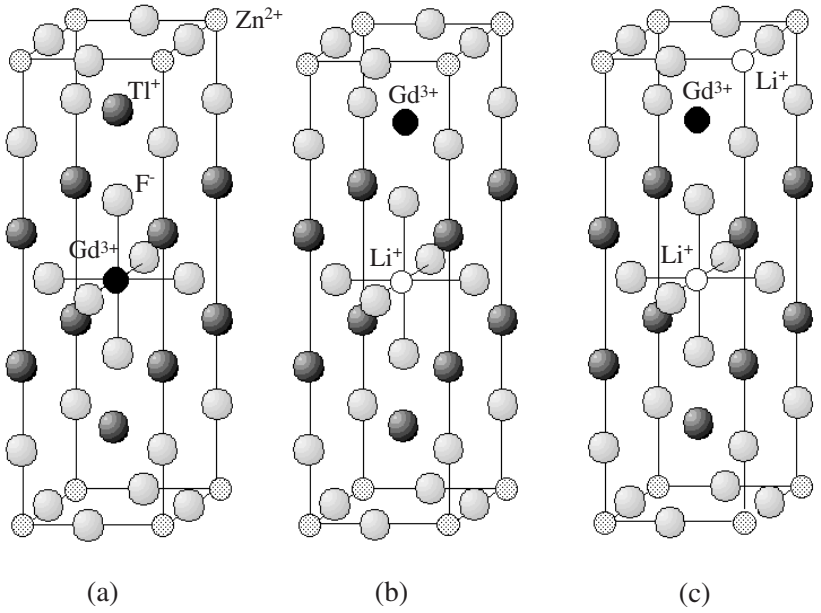

Figure 6. Schematic models of the local environments for (a) the A centre, (b) the B centre and (c) the C centre.

cubic and axial parameters for the B centre are quite different from those for other centres where Gd^{3+} ions substitute for divalent cation sites in six-fold coordination, as seen from table 3. Especially, the b_{6c} parameter for the B centre is very small. This indicates that the substitutional site of Gd^{3+} for the B centre differs from that for the A centre. As mentioned in section 3, signals from the A centre disappear in the crystals co-doped with Gd^{3+} and Li^+. This suggests that the Li^+ ions prevent the formation of the A centre. In crystals of $RbZnF_3$ co-doped with Gd^{3+} and Li^+, new signals from the Gd^{3+}–Li^+ pair replacing a Zn^{2+}–Zn^{2+} bond were observed in place of those in crystals doped only with Gd^{3+}, where the Gd^{3+}–Li^+ pairs were related to the formation of the hexagonal structure in the matrix [13]. In Tl_2ZnF_4, preferential occupation of a Li^+ ion may occur at the Zn^{2+} site and may prevent substitution of a Gd^{3+} ion for the Zn^{2+} site forming a Gd^{3+}–Li^+ pair, similar to that in $RbZnF_3$. So, we conclude that the Gd^{3+} for the B centre substitutes for Tl^+. The B centre may be ascribed to a substitutional Gd^{3+} ion at a Tl^+ ion in nine-fold coordination with association of a Li^+ ion at the second-nearest Zn^{2+} site along the c axis. A schematic model of the B centre is shown in figure 6(b). This may be the first EPR observation of the Gd^{3+} ion in nine-fold coordination.

It has been shown by Kiel [19] that the odd terms of the crystal field give rise to contributions to the fine-structure splitting in second order. Bijvank *et al* [20] applied the second-order effects of the odd-crystal field to the analysis of the values of the parameters b_2^0 determined by EPR experiments of Gd^{3+}–M^+ complexes in CaF_2-like crystals, where the contribution to b_2^0 from the odd-crystal field was estimated as a considerable opposite effect against that from the even-crystal fields. The tetragonal centres A and B are formed in the same host Tl_2ZnF_4 crystal with the same-order magnitude of b_2^0 ($= b_{2a}$). The odd-crystal field effects to the b_{2a} is expected for the B centre in nine-fold coordination with a lack of inversion symmetry, in contrast with the case for the A centre in the six-fold coordination with inversion symmetry.

Table 4. Fine-structure parameters b_{na} ($n = 2, 4$) and their ratios of b_{4a}/b_{2a} for the Gd^{3+} A and B centres in Tl_2ZnF_4 together with those for the uncompensated Gd^{3+} centres (I centre) in other layered perovskite fluorides and those for the Gd^{3+}–V_M centres in perovskite fluorides. The last column denotes the existence of inversion symmetry (○) and lack of inversion symmetry (×) of the centres. Units of b_{na} are in 10^{-4} cm^{-1}.

Crystal	Centre	b_{2a}	b_{4a}	b_{4a}/b_{2a}	Coordination	Inversion
Tl_2ZnF_4	A	−557.6	5.78	−0.0104	6	○
	B	−288.9	8.36	−0.0289	9	×
Rb_2CdF_4 [1]	I	−549.9	5.25	−0.0095	6	○
Cs_2CdF_4 [1]	I	−443.0	6.55	−0.0148	6	○
$RbZnF_3$ [13]	Gd^{3+}–V_{Rb}	−347.6	10.14	−0.0292	12	×
$RbCdF_3$ [3]	Gd^{3+}–V_{Cd}	−291.3	6.20	−0.0213	6	×
$RbCaF_3$ [3]	Gd^{3+}–V_{Ca}	−274.9	5.72	−0.0208	6	×
$CsCdF_3$ [3]	Gd^{3+}–V_{Cd}	−315.1	6.90	−0.0219	6	×
$CsCaF_3$ [3]	Gd^{3+}–V_{Ca}	−314.7	6.91	−0.0220	6	×

The ratio of b_{4a}/b_{2a} for the B centre is compared with that for the A centre. The magnitude of the ratio for the B centre is about three times larger than that for the A centre as seen from table 4. In this table the ratios of b_{4a}/b_{2a} are listed for several centres having the same order of magnitude of b_2^0 in perovskite fluorides. The ratios for the I centre in layered perovskite fluorides with inversion symmetry are also compared with those for the tetragonal centres in six- and twelve-fold coordinations with lack of inversion symmetry in perovskite fluorides. The magnitudes of the ratio for the centres with inversion symmetry are smaller than those for the centres which lack inversion symmetry. The larger magnitude of the ratio for the centres with lack of inversion symmetry may be due to reduction of the magnitude of b_{2a} by the odd-crystal field effects. The term in b_{4a} denotes the uniaxial character of higher order about the tetragonal axis. This result suggests that the odd-crystal fields may be expected to be more effective to the b_{2a} than the b_{4a}. The ratio of b_{4a}/b_{2a} may be applied as the empirical information on the presence of inversion symmetry for tetragonal Gd^{3+} centres.

4.2. Monoclinic centre C

As seen from figure 2 signals from the C centre were observed for the crystals co-doped with Gd^{3+} and Li^+ in place of those for the A centre. This result suggests the preferential occupation of Li^+ at the Zn^{2+} site. For the tetragonal B centre, excess divalent positive charge on the Gd^{3+} ion at a Tl^+ site is compensated locally by a Li^+ ion at the second-nearest Zn^{2+} site along the c axis. For the monoclinic C centre the Gd^{3+} ion can be expected to substitute for Tl^+ ion, similar to the case for the B centre.

The principal z axis of the fine-structure terms for the C centre is declined by 40.3° from the c axis in the $(\bar{1}10)$ plane, as seen in table 2. Around the Gd^{3+} ion at the Tl^+ site there exist the nearest four Zn^{2+} ions in its neighbourhood along the ⟨111⟩ directions as shown in figure 1(b). For the C centre, another association of a Li^+ ion at one of the nearest Zn^{2+} sites in the $(\bar{1}10)$ plane may be expected. A schematic model of the C centre is shown in figure 6(c).

For charge-compensated centres formed in layered perovskite fluorides, the relationship between the fine-structure parameters b_2^m ($m = 0, 2$) and local environment around the Gd^{3+} ion was analysed using the spin Hamiltonian separation method by separating the fine-structure terms in the spin Hamiltonian into two uniaxial terms along the c axis and along the direction to the charge compensator.

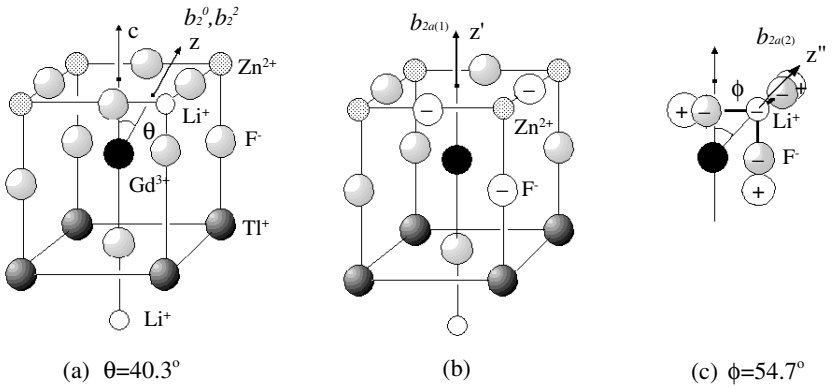

Figure 7. A schematic representation of the spin Hamiltonian separation analysis for the C centre by assuming distortions of ligand close to Li^+ at the nearest Zn^{2+} site. Spin Hamiltonian separation corresponds to the separation of the configuration for the C centre shown in (a) into the configurations shown in (b) and (c). Effects of the assumed undistorted ligands labelled by '−' in (b) are cancelled out by superposition of ligands labelled '+' in (c). The configuration (b) is comparable with that for the B centre and the configuration (c) denotes the uniaxial one caused by the Li^+-charge compensator at the nearest Zn^{2+} site. Signs in (c) denote the effective charge relative to the matrix crystal.

The spin Hamiltonian separation analysis for the C centre corresponds to the *separation* of the configuration for the C centre into two axial configurations with axial parameters $b_{2a(1)}$ and $b_{2a(2)}$. The separation is schematically shown in figure 7, assuming that the local distortions of the F^- ions close to the charge compensator take place. The configuration for the centre C in figure 7(a) is composed of superposition of the configurations in figures 7(b) and (c). The configuration for the axial parameter $b_{2a(1)}$ is deduced by assuming the undistorted ligands as shown in figure 7(b). This configuration is comparable with that for the tetragonal B centre. The other configuration for the axial parameter $b_{2a(2)}$ is shown in figure 7(c). This configuration is composed of the distorted ligands, a Li^+ charge compensator and additional ligands to cancel the undistorted ligands assumed in figure 7(b) by superposition of the configurations. In the framework of the approximation that the direction to the Li^+ is assumed to be declined by 54.7° from the c axis, the configuration in figure 7(c) denotes the axial one along the [111] direction with the parameter $b_{2a(2)}$.

Here, we try to separate the fine structure terms into two uniaxial terms as follows:

$$b_2^0 O_2^0(z) + b_2^2 O_2^2(x, y) = b_{2a(1)} O_2^0(z') + b_{2a(2)} O_2^0(z''), \tag{6}$$

where the z' axis is parallel to the c axis and the z'' axis is assumed to be declined by 54.7° from the c axis in the $(\bar{1}10)$ plane. Using the transformation properties of the Stevens operators given by Rudowicz [21], we can deduce the following conditions that satisfy equation (6):

$$b_{2a(1)} = \frac{b_2^0}{2}(3\cos^2\theta - 1) + \frac{b_2^2}{2}\sin^2\theta, \tag{7}$$

$$b_{2a(2)} = \frac{3b_2^0}{2}\sin^2\theta + \frac{b_2^2}{2}(\cos^2\theta + 1), \tag{8}$$

and

$$\sin 2\theta = \frac{2\sqrt{2}b_{2a(2)}}{3b_2^0 - b_2^2}. \tag{9}$$

Table 5. Separated parameters $b_{2a(1)}$ and $b_{2a(2)}$ for the C centre with monoclinic symmetry together with b_2^0 for the A and B centres with tetragonal symmetry observed in Tl_2ZnF_4. The parameters b_2^0 for the trigonal and tetragonal Gd^{3+} centres of several kinds reported in some perovskite fluorides are listed for comparison. Units of the parameters are in 10^{-4} cm^{-1}.

Crystal	Centre	$b_{2a(1)}$	$b_{2a(2)}$	b_2^0	Site	Symmetry
Tl_2ZnF_4	C	−227.4	−495.0	—	Tl^+	Monoclinic
	B	—	—	−288.9	Tl^+	Tetragonal
	A	—	—	−557.6	Zn^{2+}	Tetragonal
$RbCaF_3$ [11]	Gd^{3+}–V_{Rb}	—	—	80.1	Ca^{2+}	Trigonal
$RbCaF_3$ [3]	Gd^{3+}–V_{Ca}	—	—	−274.9	Ca^{2+}	Tetragonal
$RbCaF_3$ [3]	Gd^{3+}–Li^+	—	—	−318.3	Ca^{2+}	Tetragonal
$RbCdF_3$ [3]	Gd^{3+}–V_{Cd}	—	—	−291.3	Cd^{2+}	Tetragonal
$RbCdF_3$ [3]	Gd^{3+}–Li^+	—	—	−330.2	Cd^{2+}	Tetragonal

We can calculate the separated axial parameters $b_{2a(1)}$ and $b_{2a(2)}$ from equations (7) and (8) using the experimental values of b_2^0, b_2^2 and θ listed in table 2. The values obtained are tabulated in table 5. The separated parameter $b_{2a(1)}$ has a value close to the b_2^0 for the B centre. This supports that the Gd^{3+} ion for the C centre substitutes for a Tl^+ site. So, the C centre may be ascribed to a Gd^{3+} ion at the Tl^+ site associated with another Li^+ ion at the nearest Zn^{2+} site as shown in figure 6(c). The excess doubly positive charge on the Gd^{3+} is locally just-compensated by two Li^+ ions at the Zn^{2+} sites; one is located at the direction declined by about 54.7° from the c axis in the $(\bar{1}10)$ plane and the other along the c axis.

If the formation of a Gd^{3+}–Li^+ pair is related to the substitution of Gd^{3+} for a Tl^+ site similar to the B centre, the C centre may be ascribed to a Gd^{3+} ion associated with only a Li^+ ion at the nearest Zn^{2+} site. In this case, the separated parameter $b_{2a(1)}$, which has a value close to the b_2^0 for the B centre, corresponds to the configuration of the uncompensated Gd^{3+} centre substituted for a Tl^+ ion.

The negative sign of the separated parameter $b_{2a(1)}$ also shows that the signs of the b_2^0 and b_2^2 can be determined to be negative, as shown in table 2. The negative sign of b_2^0 in table 2 was confirmed from the spectrum observed with $\boldsymbol{H} \parallel z$ at 4.2 K by the depopulation effect. The sign of the angle θ in table 2 can be determined to be positive from equation (9). The negative value of $b_{2a(2)}$ is consistent with the positive sign of θ, since $3b_2^0 - b_2^2 < 0$.

The $b_{2a(2)}$ parameter is compared with b_2^0 for the Gd^{3+}–V_{Rb} centre in cubic perovskite $RbCaF_3$ crystals [11], where a vacancy at the nearest Rb^+ site along the [111] direction is associated with a charge compensator. It is known that the sign of b_{2a} is related to the sign of the effective charge along the principal z axis relative to the matrix crystal. For the trigonal centre with the charge compensator along the [111] axis, the local distortion of ligands due to the charge compensator produces the additional effective charge along the [111] axis. The effective positive charge is produced by the deviation of the ligands away from the [111] axis. The positive value of b_2^0 for the Gd^{3+}–V_{Rb} centre in $RbCaF_3$ [11] shows that the effective positive charge by the deviation of the ligands overcomes the effective negative charge due to the Rb^+ vacancy. On the other hand, the separated parameter $b_{2a(2)}$ for the C centre has the large magnitude negative value, as seen from table 5. The result suggests that the effective negative charge is produced by the distortions of the ligands for the C centre, contrary to the positive one for the Gd^{3+}–V_{Rb} centre in $RbCaF_3$ [11].

For the C centre, the ligands may deviate *toward the* [111] *axis*, as seen from figure 7(c), by the substitution of a Li^+ ion at the Zn^{2+} site due to the small ionic radius of the Li^+ ion, although the effective charge on the Li^+ ion at the Zn^{2+} site is negative. The result indicates

that the Li^+ ion may tend to form a LiF_6 complex by its nearest F^- ions. In ABF_3 crystals, the magnitudes of b_2^0 for the Gd^{3+}–Li^+ centre with a monovalent charge compensator by a Li^+ ion at the nearest B^{2+} site were observed to be larger than those for the Gd^{3+}–V_B centre with a divalent charge compensator by a B^{2+} vacancy at the same B^{2+} site, as seen in table 5. The effective negative charge increased by the Li^+ ion observed for the C centre may make the magnitude of b_2^0 for the Gd^{3+}–Li^+ centre larger than that for the Gd^{3+}–V_B centre, although the effective negative charge on the Li^+ ion is half of that on the vacancy at the nearest B^{2+} site.

5. Conclusion

In crystals doped only with Gd^{3+}, the tetragonal centre observed is identified as the uncompensated Gd^{3+} centre at a Zn^{2+} site in six-fold coordination with inversion symmetry. In crystals co-doped with Gd^{3+} and Li^+ other tetragonal and monoclinic centres are observed in place of the uncompensated centre in Gd^{3+}-only doped crystals. This result suggests that the preferential occupation of Li^+ at the Zn^{2+} site occurs in co-doped crystals. The tetragonal centre in co-doped crystals are ascribed to Gd^{3+} substituted for Tl^+ in nine-fold coordination with lack of inversion symmetry, where the divalent excess positive charge on a Gd^{3+} ion is compensated by a Li^+ ion at the neighbouring Zn^{2+} site on the c axis. The ratio of b_{4a}/b_{2a} for the tetragonal centres with lack of inversion symmetry is found to have larger magnitude than those with inversion symmetry. The larger magnitude of the ratio for the centre with lack of inversion symmetry may be related to the reduction of the magnitude of b_{2a} by the odd-crystal field effects. The result suggests that the ratio of b_{4a}/b_{2a} may be applied as empirical information on the presence of inversion symmetry for tetragonal Gd^{3+} centres.

For the monoclinic centre, another association with a Li^+ ion at the nearest Zn^{2+} site along the [111] direction is found using the spin Hamiltonian separation analysis. The separated parameter $b_{2a(2)}$ has the large magnitude negative value, in contrast with the positive one of b_2^0 for the trigonal Gd^{3+} centre associated with a vacancy at the nearest Rb^+ site along the [111] direction in cubic perovskite $RbCaF_3$ crystals. The negative value suggests that the effective charge by the distortion of the ligands becomes negative similar to that of the Li^+ ion at the Zn^{2+} site. The ligands may deviate toward the [111] axis by the substitution of a Li^+ ion at the Zn^{2+} site due to smaller ionic radius of the Li^+ ion, although the effective charge on the Li^+ ion substituted for the Zn^{2+} site is negative. The result indicates that the Li^+ ion may tend to form a LiF_6 complex by its nearest F^- ions.

References

[1] Takeuchi H, Arakawa M and Ebisu H 1987 *J. Phys. Soc. Japan* **56** 4571
Takeuchi H, Arakawa M and Ebisu H 1990 *J. Phys. Soc. Japan* **59** 2297 (erratum)
[2] Arakawa M, Ebisu H and Takeuchi H 1996 *J. Phys.: Condens. Matter* **8** 11299
[3] Arakawa M, Aoki H, Takeuchi H, Yosida T and Horai K 1982 *J. Phys. Soc. Japan* **51** 2459
[4] Arakawa M, Ebisu H and Takeuchi H 1985 *J. Phys. Soc. Japan* **54** 3577
[5] Buzaré J Y, Fayet-Bonnel M and Fayet J C 1981 *J. Phys.: Condens. Matter* **14** 67
[6] Newman D J and Urban W 1972 *Adv. Phys.* **24** 793
[7] Newman D J and Betty Ng 1989 *Rep. Prog. Phys.* **52** 699
[8] Takeuchi H, Arakawa M, Ebisu H, Tanaka H and Abe H 1998 *Proc. APES'97: 1st Asia-Pacific EPR/ESR Symp.* (Singapore: Springer) p 534
[9] Arakawa M, Ebisu H, Yosida T and Horai K 1979 *J. Phys. Soc. Japan* **46** 1483
[10] Arakawa M 1979 *J. Phys. Soc. Japan* **47** 523
[11] Takeuchi H, Ebisu H and Arakawa M 1995 *J. Phys.: Condens. Matter* **7** 1417
[12] Abraham M M, Finch C B, Kolopus J L and Lewis J T 1971 *Phys. Rev.* B **3** 2855
[13] Arakawa M, Ebisu H and Takeuchi H 1997 *J. Phys.: Condens. Matter* **9** 5193

[14] Babel D 1967 *Struct. Bonding* **3** 1
[15] Arakawa M, Ebisu H and Takeuchi H 2002 *J. Phys.: Condens. Matter* **14** 8613
[16] Abragam A and Bleaney B 1970 *Electron Paramagnetic Resonance of Transition Ions* (Oxford: Clarendon)
[17] Schrama A H M 1973 *Physica* **68** 279
[18] Arakawa M, Ebisu H and Takeuchi H 2002 *Proc. APES'01: 3rd Asia-Pacific EPR/ESR Symp.* (Amsterdam: Elsevier Science) p 219
[19] Kiel A 1966 *Phys. Rev.* **148** 249
[20] Bijvank E J, den Hartog H W and Andriessen J 1977 *Phys. Rev.* B **16** 1008
[21] Rudowicz C 1985 *J. Phys. C: Solid State Phys.* **18** 1415